Earth and Planetary Science Letters 290 (2010) 438–447

Contents lists available at ScienceDirect

Earth and Planetary Science Letters

journal homepage: www.elsevier.com/locate/epsl

Temporal variations in Pb isotopes and trace element concentrations within Chinese eolian deposits during the past 8 Ma: Implications for provenance change

Jimin Sun [a,*], Xiangkun Zhu [b]

[a] Key Laboratory of Cenozoic Geology and Environment, Institute of Geology and Geophysics, Chinese Academy of Sciences, P. O. Box 9825, Beijing 100029, China
[b] Laboratory of Isotope Geology, MLR, Institute of Geology, Chinese Academy of Geological Sciences, Beijing 100037, China

ARTICLE INFO

Article history:
Received 4 July 2009
Received in revised form 15 December 2009
Accepted 4 January 2010
Available online 25 January 2010

Editor: P. DeMenocal

Keywords:
eolian dust
provenance
Loess Plateau
glacial history
geochemistry

ABSTRACT

The Pb isotopes and trace element compositions of the silicate fraction of airborne dust from the Chinese Loess Plateau were analyzed to infer provenance change during the past 8 Ma. The results indicate that the composition of eolian dust changed at 2.6 Ma, coincident with initiation of the Northern Hemisphere ice sheet. The change in trace element composition at 2.6 Ma indicates that a larger component of the eolian dust was derived from felsic rocks after this time. Pb isotopic evidence demonstrates that the source material of Tertiary Red Clay differs to some extent from that of Quaternary eolian deposits. Although chemical weathering may result in compositional changes in eolian deposits, such a scenario is not supported by the present evidence. Given that glacial grinding and frost-weathering processes have been active in the peaks of high mountains during the Quaternary, eolian dust of this age contains a large proportion of material derived from areas of high topographic relief and relatively little material from low-lying cratonic regions. Such alpine processes played an important role in controlling the distinct changes in Pb isotopes and trance element concentrations recorded at around 2.6 Ma.

1. Introduction

Windblown deposits provide insights into paleoclimatic change (Liu, 1985; Pye, 1987; Kukla and An, 1989; Derbyshire et al., 1998). In the past two decades, a variety of climatic proxies have been used to reconstruct paleoclimatic changes on the Loess Plateau, China (Heller and Liu, 1984; Liu, 1985; Ding et al., 1994; Chen et al., 1999; Ji et al., 2004). Compared with the large amount of paleoclimate research, few studies have considered the provenance of Chinese loess. Based on case studies of modern dust storms (Liu et al., 1981; Liu, 1985; Sun et al., 2000, 2001) and geochemical/isotopic analyses of loess deposits (Sun, 2002), Chinese loess is thought to be derived from Gobi (stony desert) and desert regions. An alternative view is that silt deflated from the surfaces of numerous, large piedmont alluvial fans in the Hexi Corridor, Gansu, made a major contribution to the loess column in the western region of the Chinese Loess Plateau (Derbyshire et al., 1998). Sun (2005) reconstructed the temporal record of Nd and Sr isotopes and inferred provenance changes from these data.

In addition to Nd and Sr isotopes, Pb isotope data can be used to reconstruct provenance changes. Previous studies on spatial and temporal variations in the Pb isotopes of eolian silicate fractions in marine deposits indicate that a large proportion of the sediment in the central Pacific Ocean is eolian deposits derived from Chinese deserts (e.g., Pettke et al., 2000; Jones et al., 2000; Godfrey, 2002; van de Flierdt et al., 2003; Stancin et al., 2006; Klemm et al., 2007). Despite the wealth of information provided by the above works, few studies have attempted to reconstruct a long-term Pb isotopic record for Chinese eolian deposits (Zhu et al., 1988).

The present paper reports on temporal variations in Pb isotopes and trace element concentrations within Chinese eolian deposits, providing new evidence for provenance change during the past 8 Ma. The present work aims to address the following questions:

(1) What is the nature of the loess-sized material produced during the Tertiary? Does Quaternary loess have a different source material to that of Tertiary eolian deposits?
(2) Eolian deposits that accumulated on the Loess Plateau were derived from upwind outwash plains or alluvial fans in mountainous areas (Sun, 2002); consequently, the loess was derived from the top surface of the crust. This point is of particular interest because analyses of temporal changes in the provenance of eolian dust provide insight into the relationship between the accumulation of such dust and the evolution of the upper crust during the late Cenozoic.

2. Materials and methods

On the Loess Plateau, Quaternary loess deposits are underlain by late Tertiary reddish eolian dust (known as Red Clay). The present study is concerned with the Jingchuan section (107°22′05″E, 35°17′

* Corresponding author. Tel.: +86 10 8299 8389; fax: +86 10 6201 0846.
E-mail address: jmsun@mail.igcas.ac.cn (J. Sun).

0012-821X/$ – see front matter © 2010 Published by Elsevier B.V.
doi:10.1016/j.epsl.2010.01.001

30″N, Fig. 1), located in the central Loess Plateau, where eolian deposits consist of Tertiary Red Clay and an overlying Quaternary loess–paleosol succession (Fig. 2) that contains 33 paleosols (S0 to S32) and 33 loess beds (L1 to L33). Paleomagnetic polarity data (Ding et al., 2001a) indicate that the lithologic boundary between the Quaternary loess and Red Clay corresponds to the Matuyama/Gauss (M/G) boundary (~2.6 Ma), while the age of the base of the Red Clay at Jingchuan is ~8 Ma (Fig. 2).

In this study, 116 samples were analyzed for Pb isotopes and 63 samples were measured for trace element contents. Because the particle size of the Red Clay is much finer than that of Quaternary loess, the isotopic and geochemical compositions of eolian deposits are dependent on grain size (Schettler et al., 2009). To minimize this grain-size effect, only the fine fraction (<20 μm) was analyzed, pipetted according to Stokes' Law. The advantages of using this fraction are as follows: (1) most of the particles within this fraction are derived from distal source regions transported over great distances, and (2) the coarse particles derived mainly from local sources are largely removed from the analysis.

Chinese loess is rich in carbonate (Liu, 1985), much of which is of secondary origin, as indicated by carbonate leaching in soil profiles (Guo and Fedoroff, 1991). Therefore, it is important to remove carbonate from the samples in order to effectively trace the provenance of the dust. The silicate fraction within each sample was refined by chemical extraction of carbonate using 2.5 N HCl leaching for 20 h, following the procedure proposed for Chinese loess by Asahara (1999), ensuring that all the carbonate in the eolian dust was eliminated. The addition of this acid also removed soluble salts, oxides, and hydroxides. The detrital residue, consisting mainly of silicates, was washed several times with deionized water and dried for further analysis.

Samples for analyses of Pb isotopes were digested using a mixture of ultrapure HF and HNO_3, followed by purification using conventional ion-exchange chromatography. Measurements of Pb isotopic compositions were performed using a Nu Instrument multi-collector ICP-MS housed at the Laboratory of Isotope Geology, the Ministry of Land and Resources of China, using a Tl-doping method similar to that described by Belshawa et al. (1998). Repeat analyses of the NBS 981 Pb isotopic standard gave a reproducibility (2δ) of $^{208}Pb/^{206}Pb = 2.1674 \pm 0.0004$, $^{207}Pb/^{206}Pb = 0.91478 \pm 0.00018$, $^{206}Pb/^{204}Pb = 16.9402 \pm 0.007$, $^{207}Pb/^{204}Pb = 15.4966 \pm 0.0030$, and $^{206}Pb/^{204}Pb = 36.7155 \pm 0.012$ ($n = 30$) at the 2SD level.

Samples for analyses of trace element concentrations were prepared using a series of steps involving acid dissolution, following the method described by Ding et al. (2001b). The finial solutions were analyzed using ICP-MS (ELEMENT, Finnigan MAT) at the State Key Laboratory of Lithospheric Evolution, Institute of Geology and Geophysics, the Chinese Academy of Sciences. The uncertainties in the analysis were less than ±5%.

3. Results

3.1. Pb isotopes

Pb isotopic compositions are summarized as a function of depth in Table 1 and Fig. 3. The obtained values of $^{206}Pb/^{204}Pb$, $^{207}Pb/^{204}Pb$, and $^{208}Pb/^{204}Pb$ fall in the ranges of 18.84–18.98, 15.67–15.70, and 39.08–39.18, respectively.

Vertical variations in Pb isotopes show two distinct patterns (Fig. 3): $^{206}Pb/^{204}Pb$ and $^{207}Pb/^{204}Pb$ change from generally high values in the Tertiary Red Clay to low values after 2.6 Ma (Fig. 3 a,b), whereas $^{208}Pb/^{204}Pb$, $^{208}Pb/^{206}Pb$, and $^{208}Pb/^{207}Pb$ show a different trend (Fig. 3c–e).

3.2. Trace elements

Trace element compositions are given in Table 2 and Fig. 4. Temporal changes in trace element contents also show two distinct patterns: Co, Ni, Cr, Cu, Zn, Pb, Zr, and Hf generally show higher values in the Red Clay and lower values after 2.6 Ma, whereas Nb, Ta, Rb, Cs, Ba, and Sr generally show lower values in the Red Clay and higher values after 2.6 Ma.

4. Discussion

4.1. Pb isotope evidence for a change in the provenance of eolian dust after 2.6 Ma

Pb isotopes can be used as tracers of change in sediment provenance (e.g., Biscaye et al., 1997; Pettke et al., 2000; Jones et al.,

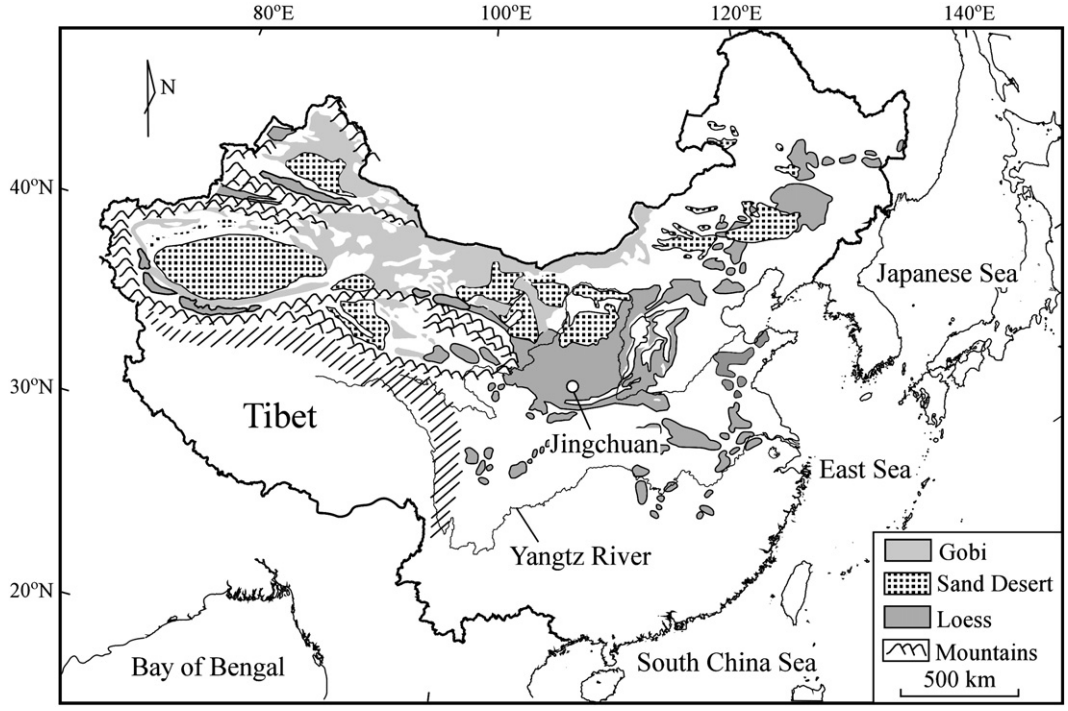

Fig. 1. Map showing the distribution of mountains, Gobi (stony desert), sand desert, and loess in China, as well as the location of the Jingchuan section analyzed in the present study.

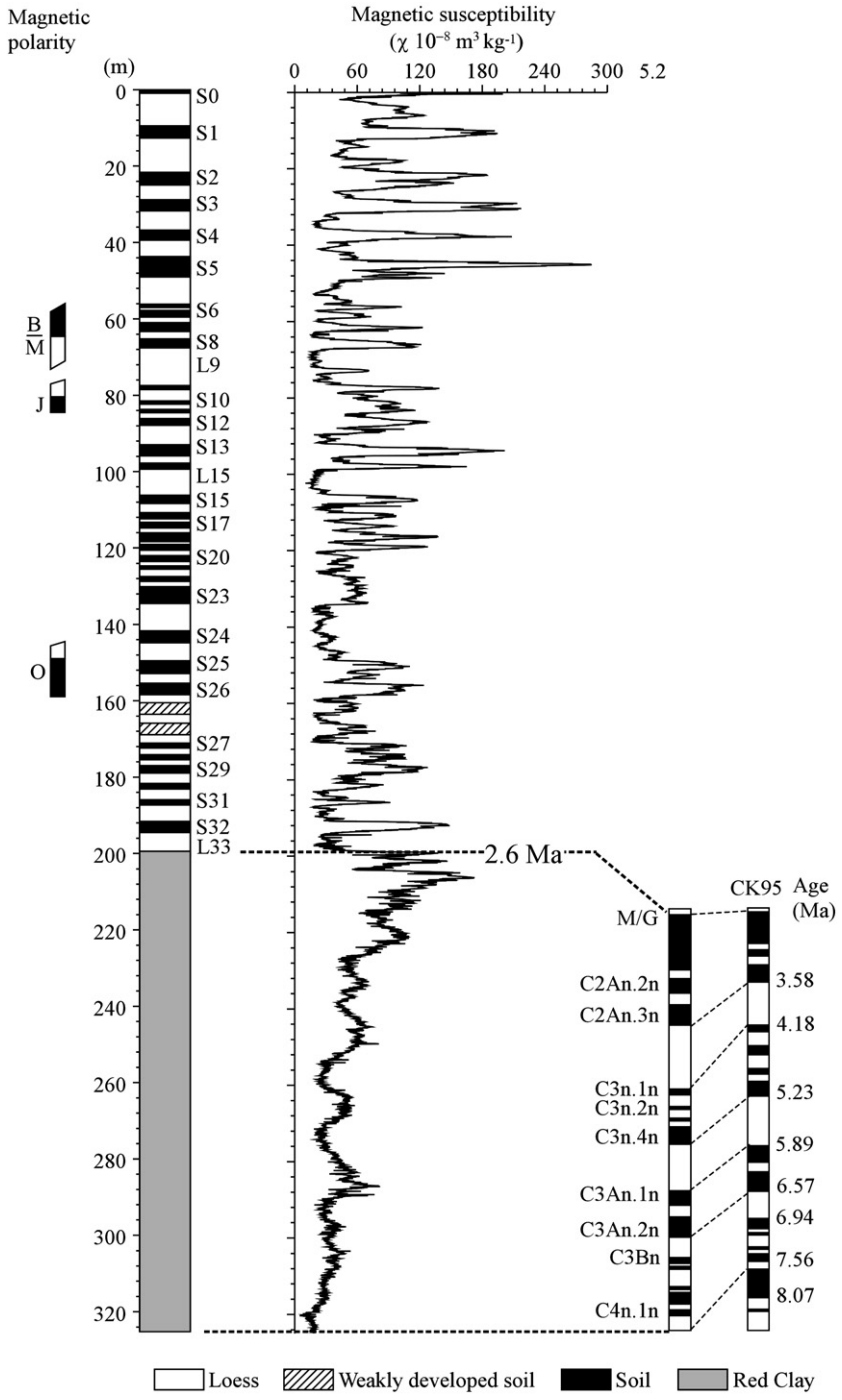

Fig. 2. Pedostratigraphy, magnetic susceptibility, and paleomagnetic polarity data (from Ding et al., 2001a) for the section at Jingchuan.

2000). In the present study, a distinct change in Pb isotopes occurred at 2.6 Ma (Fig. 3): the Tertiary Red Clay contains more radiogenic ^{207}Pb and ^{206}Pb, and less radiogenic ^{208}Pb compared with Quaternary eolian deposits (Fig. 3a–c). These changes in Pb isotopes at 2.6 Ma are interpreted to represent a change in the provenance of dust, consistent with provenance changes inferred from long-term variations in Sr and Nd isotopes (Sun, 2005).

The above changes in dust provenance are also apparent on plots of $^{207}Pb/^{204}Pb$ versus $^{206}Pb/^{204}Pb$ and $^{208}Pb/^{204}Pb$ versus $^{206}Pb/^{204}Pb$ (Fig. 5), which reveal that most of the samples of Tertiary Red Clay plot in a different group from the samples of Quaternary loess–soil, suggesting that the source of dust within the Red Clay is to some extent different from that within the Quaternary eolian dust. This finding is supported by the fact that the two groups of samples also plot in different fields in diagrams of $^{87}Sr/^{86}Sr$ versus $^{208}Pb/^{206}Pb$, and $^{87}Sr/^{86}Sr$ versus $^{207}Pb/^{204}Pb$ (Fig. 6).

4.2. Trace element evidence for a change in the provenance of eolian dust at 2.6 Ma

Trace element data provide a useful indication of source rock type. Of the elements in the present study that show a marked decrease after 2.6 Ma (Co, Ni, Cr, Cu, Zn, Pb, Zr, and Hf), Co, Ni, Cr, Cu, and Zn are transition elements. Co and Ni have similar geochemical behaviors, and are more strongly concentrated in basic rocks than in granitic rocks (Mielke, 1979). Cr is strongly oxyphilic in the upper crust. In the

Table 1
Pb isotopic data for the Quaternary loess–paleosol and the Tertiary Red Clay at Jingchuan.

Depth (m)	Lithology	Unit	$^{208}Pb/^{204}Pb$	$^{207}Pb/^{204}Pb$	$^{206}Pb/^{204}Pb$	$^{208}Pb/^{206}Pb$	$^{207}Pb/^{206}Pb$	$^{208}Pb/^{207}Pb$
5.3	Loess	L1	39.10042	15.67374	18.85291	2.07397	0.83137	2.49465
10.75	Soil	S1	39.12023	15.67701	18.86248	2.07397	0.83112	2.49539
21.65	Soil	S2	39.15378	15.67678	18.89528	2.07215	0.82967	2.49757
27.4	Loess	L3	39.11961	15.67359	18.87793	2.07224	0.83026	2.49589
30.65	Soil	S3	39.16470	15.67864	18.90162	2.07203	0.82949	2.49797
33.7	Loess	L4	39.11022	15.67454	18.87349	2.07223	0.83051	2.49514
37.75	Soil	S4	39.15029	15.67777	18.88753	2.07281	0.83006	2.49718
41.45	Loess	L5	39.11301	15.67587	18.87654	2.07204	0.83044	2.49511
45.15	Soil	S5	39.17134	15.68078	18.89497	2.07311	0.82989	2.49805
56.15	Soil	S6	39.09407	15.67469	18.86219	2.07262	0.83101	2.49409
59.1	Loess	L7	39.12911	15.67584	18.87436	2.07314	0.83054	2.49614
61.6	Soil	S7	39.08683	15.67341	18.83748	2.07495	0.83203	2.49383
63.6	Loess	L8	39.13612	15.67701	18.89198	2.07157	0.82982	2.49640
71.6	Loess	L9	39.11779	15.68066	18.89814	2.06993	0.82975	2.49465
77.5	Soil	S9	39.16225	15.68398	18.91524	2.07041	0.82917	2.49696
80.35	Loess	L10	39.16043	15.68556	18.92611	2.06912	0.82878	2.49659
81.45	Soil	S10	39.17702	15.68370	18.92280	2.07036	0.82883	2.49794
82.5	Loess	L11	39.15976	15.68507	18.93463	2.06816	0.82838	2.49663
83.25	Soil	S11	39.15509	15.68428	18.91796	2.06973	0.82907	2.49646
84.85	Loess	L12	39.12988	15.68053	18.90130	2.07022	0.82960	2.49544
86.55	Soil	S12	39.15770	15.68188	18.90827	2.07093	0.82937	2.49700
89.85	Loess	L13	39.09341	15.67501	18.87940	2.07069	0.83027	2.49400
96.25	Loess	L14	39.10338	15.67267	18.89569	2.06943	0.82943	2.49500
98	Soil	S14	39.16104	15.67855	18.90062	2.07194	0.82953	2.49775
101.95	Loess	L15	39.11070	15.67475	18.88726	2.07075	0.82991	2.49514
106.85	Soil	S15	39.15306	15.67845	18.91640	2.06980	0.82883	2.49725
108.95	Loess	L16	39.13757	15.67914	18.88956	2.07191	0.83004	2.49616
110.85	Soil	S16	39.12735	15.67423	18.89189	2.07112	0.82968	2.49628
112.45	Loess	L17	39.11166	15.67346	18.87849	2.07176	0.83023	2.49541
113.65	Soil	S17	39.13638	15.67760	18.89263	2.07152	0.82983	2.49633
115.1	Loess	L18	39.13214	15.67510	18.89916	2.07058	0.82941	2.49645
116.35	Soil	S18	39.13144	15.67302	18.88062	2.07257	0.83011	2.49674
117.85	Loess	L19	39.11520	15.67244	18.87715	2.07209	0.83023	2.49580
120.5	Loess	L20	39.12925	15.67849	18.88438	2.07204	0.83024	2.49573
121.75	Soil	S20	39.11749	15.67378	18.87860	2.07205	0.83024	2.49573
123.3	Loess	L21	39.11808	15.67410	18.87857	2.07209	0.83026	2.49571
123.95	Soil	S21	39.13901	15.67733	18.89113	2.07182	0.82988	2.49653
125.9	Loess	L22	39.11890	15.67455	18.88775	2.07113	0.82988	2.49570
127.05	Soil	S22	39.16551	15.68002	18.91911	2.07016	0.82879	2.49780
129.15	Loess	L23	39.13797	15.67529	18.89630	2.07120	0.82954	2.49679
131.05	Soil	S23	39.15028	15.67718	18.89975	2.07147	0.82949	2.49728
138.05	Loess	L24	39.10851	15.67332	18.87478	2.07200	0.83038	2.49523
142.75	Soil	S24	39.11089	15.67138	18.88026	2.07152	0.83004	2.49569
146.7	Loess	L25	39.13949	15.67645	18.89645	2.07126	0.82960	2.49671
150.3	Soil	S25	39.13128	15.67483	18.90266	2.07015	0.82924	2.49644
153.3	Loess	L26	39.12947	15.67329	18.89828	2.07053	0.82935	2.49657
155.1	Soil	S26	39.14139	15.67525	18.89788	2.07121	0.82947	2.49702
161.85	Loess	L27	39.10373	15.66827	18.87871	2.07131	0.82994	2.49573
166.1	Soil	S27	39.14114	15.67684	18.90281	2.07065	0.82934	2.49675
166.85	Loess	L28	39.13182	15.67497	18.89388	2.07114	0.82963	2.49645
167.25	Soil	S28	39.11804	15.67297	18.88821	2.07103	0.82977	2.49589
169.35	Loess	L29	39.13740	15.67796	18.89210	2.07163	0.82987	2.49633
171.1	Soil	S29	39.15357	15.68192	18.90409	2.07117	0.82955	2.49673
172.65	Loess	L30	39.09073	15.66926	18.86516	2.07211	0.83059	2.49474
174.5	Soil	S30	39.14700	15.67821	18.89891	2.07139	0.82958	2.49690
175.55	Loess	L31	39.15027	15.67806	18.91260	2.07006	0.82897	2.49714
176.75	Soil	S31	39.14864	15.68172	18.89872	2.07150	0.82978	2.49645
184.9	Loess	L32	39.11963	15.67437	18.88365	2.07161	0.83005	2.49577
191.8	Soil	S32	39.15286	15.68001	18.90903	2.07059	0.82923	2.49699
196.45	Loess	L33	39.16569	15.68403	18.93764	2.06814	0.82819	2.49717
206.25	Red clay	RC	39.13046	15.68910	18.94585	2.06538	0.82810	2.49412
207.5	Red clay	RC	39.12333	15.68806	18.93826	2.06584	0.82838	2.49383
210	Red clay	RC	39.11458	15.68654	18.92936	2.06634	0.82869	2.49351
211.25	Red clay	RC	39.15009	15.69269	18.95070	2.06589	0.82808	2.49480
213.75	Red clay	RC	39.16152	15.69932	18.96750	2.06466	0.82770	2.49447
217.5	Red clay	RC	39.13966	15.68903	18.95132	2.06527	0.82786	2.49472
218.75	Red clay	RC	39.14450	15.69037	18.96177	2.06439	0.82747	2.49481
221.25	Red clay	RC	39.14202	15.69025	18.94595	2.06598	0.82816	2.49467
222.5	Red clay	RC	39.13847	15.68628	18.94250	2.06617	0.82810	2.49508
226.25	Red clay	RC	39.16453	15.69278	18.97801	2.06368	0.82689	2.49570
227.5	Red clay	RC	39.15104	15.69239	18.94649	2.06640	0.82825	2.49491
228.75	Red clay	RC	39.11145	15.68866	18.90798	2.06852	0.82974	2.49298
230	Red clay	RC	39.12742	15.69431	18.91330	2.06878	0.82980	2.49310
232.5	Red clay	RC	39.11892	15.69303	18.91514	2.06813	0.82965	2.49276

(continued on next page)

Table 1 (*continued*)

Depth (m)	Lithology	Unit	$^{208}Pb/^{204}Pb$	$^{207}Pb/^{204}Pb$	$^{206}Pb/^{204}Pb$	$^{208}Pb/^{206}Pb$	$^{207}Pb/^{206}Pb$	$^{208}Pb/^{207}Pb$
233.75	Red clay	RC	39.07606	15.68408	18.87712	2.07002	0.83085	2.49145
235	Red clay	RC	39.09452	15.69091	18.89405	2.06914	0.83047	2.49154
237.5	Red clay	RC	39.13248	15.69325	18.93459	2.06672	0.82881	2.49359
238.75	Red clay	RC	39.11188	15.68854	18.93357	2.06574	0.82861	2.49302
241.25	Red clay	RC	39.11852	15.68976	18.92013	2.06756	0.82926	2.49325
242.5	Red clay	RC	39.10285	15.68880	18.90647	2.06823	0.82981	2.49241
245	Red clay	RC	39.11275	15.69362	18.91196	2.06815	0.82983	2.49227
246.25	Red clay	RC	39.08836	15.68567	18.89829	2.06835	0.83000	2.49198
250	Red clay	RC	39.10859	15.68846	18.88589	2.07078	0.83070	2.49282
252.5	Red clay	RC	39.07963	15.67832	18.87567	2.07037	0.83061	2.49259
253.75	Red clay	RC	39.10991	15.68729	18.89467	2.06989	0.83025	2.49310
256.25	Red clay	RC	39.08755	15.68708	18.88843	2.06939	0.83051	2.49170
257.5	Red clay	RC	39.11666	15.68759	18.89422	2.07030	0.83028	2.49348
260	Red clay	RC	39.09126	15.68582	18.88219	2.07027	0.83072	2.49214
261.25	Red clay	RC	39.12746	15.69217	18.90205	2.07001	0.83018	2.49344
265	Red clay	RC	39.09771	15.68504	18.88104	2.07074	0.83073	2.49267
267.5	Red clay	RC	39.10290	15.68879	18.87815	2.07133	0.83106	2.49241
268.75	Red clay	RC	39.11702	15.68918	18.90872	2.06873	0.82973	2.49325
271.25	Red clay	RC	39.08791	15.68644	18.88266	2.07004	0.83073	2.49183
272.5	Red clay	RC	39.13458	15.68885	18.92404	2.06798	0.82904	2.49442
273.75	Red clay	RC	39.12016	15.68567	18.91362	2.06836	0.82933	2.49401
278.75	Red clay	RC	39.13520	15.69332	18.93167	2.06718	0.82895	2.49375
280	Red clay	RC	39.11275	15.68840	18.90624	2.06877	0.82980	2.49310
282.5	Red clay	RC	39.11341	15.68499	18.91822	2.06750	0.82909	2.49368
283.75	Red clay	RC	39.14246	15.68875	18.93923	2.06674	0.82837	2.49494
286.25	Red clay	RC	39.12740	15.68619	18.93342	2.06658	0.82849	2.49439
287.5	Red clay	RC	39.11812	15.68457	18.92584	2.06692	0.82874	2.49405
291.25	Red clay	RC	39.12710	15.68441	18.91987	2.06804	0.82899	2.49465
293.75	Red clay	RC	39.13826	15.69132	18.94035	2.06640	0.82846	2.49426
296.25	Red clay	RC	39.14264	15.69300	18.93406	2.06731	0.82882	2.49427
300	Red clay	RC	39.14627	15.69232	18.95047	2.06572	0.82807	2.49461
301.25	Red clay	RC	39.14130	15.69110	18.94682	2.06585	0.82817	2.49449
303.75	Red clay	RC	39.12311	15.68732	18.92543	2.06722	0.82890	2.49393
305	Red clay	RC	39.13352	15.69128	18.93489	2.06674	0.82870	2.49397
307.5	Red clay	RC	39.12148	15.68511	18.93000	2.06664	0.82858	2.49418
308.75	Red clay	RC	39.10013	15.68244	18.91317	2.06735	0.82918	2.49324
311.25	Red clay	RC	39.14945	15.68954	18.93281	2.06781	0.82870	2.49526
312.5	Red clay	RC	39.12950	15.68569	18.91684	2.06850	0.82919	2.49460
315	Red clay	RC	39.12887	15.69241	18.93472	2.06651	0.82876	2.49349
316.25	Red clay	RC	39.11394	15.68334	18.92100	2.06722	0.82889	2.49398

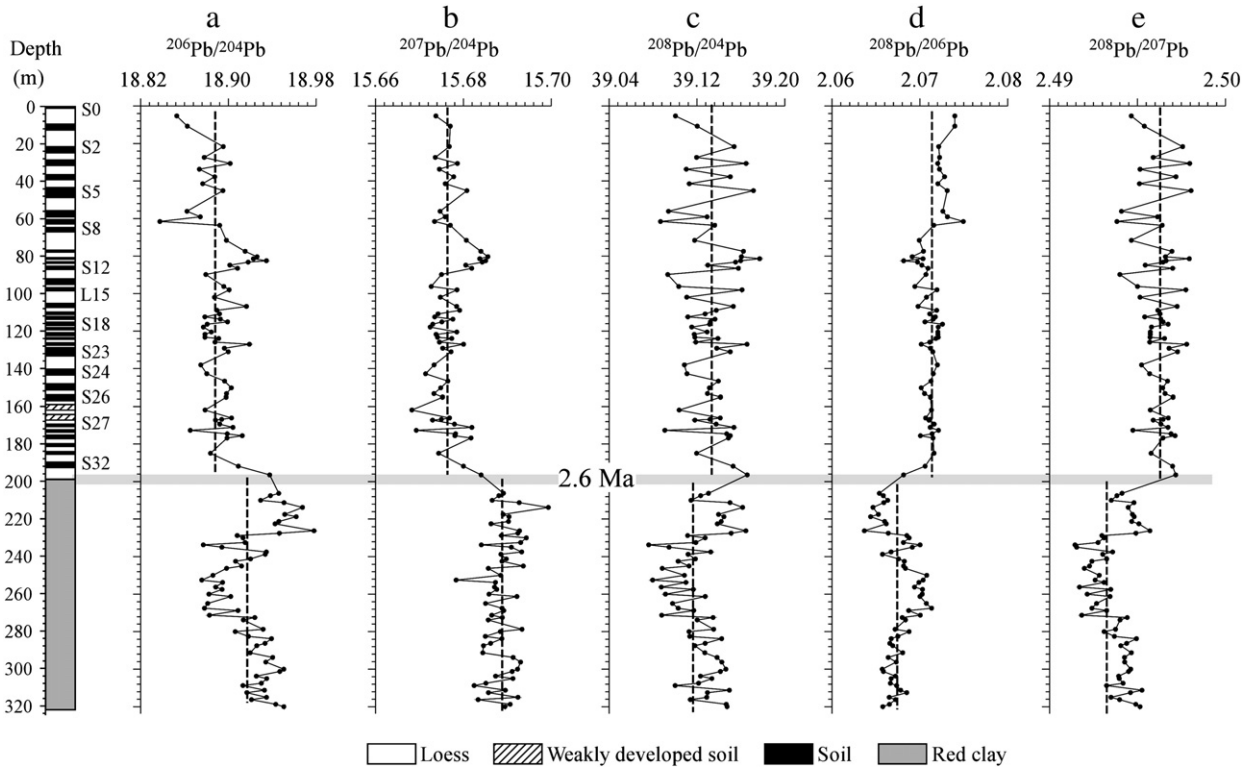

Fig. 3. Temporal variations in Pb isotope ratios for the Jingchuan section. Note the distinct changes in Pb isotope ratios at 2.6 Ma.

Table 2
Trace element concentrations for the Quaternary loess–paleosol and the Tertiary Red Clay at Jingchuan.

Depth (m)	Co	Ni	Cr	Cu	Zn	Pb	Zr	Hf	Nb	Ta	Rb	Cs	Ba	Sr
0.4	8.2	32.2	84.2	24.8	54.9	9.2	181	5.4	16.7	1.41	70.7	11.6	357	74.1
16.6	8.6	30.8	82.8	26.0	55.0	8.8	177	5.4	18.0	1.35	67.1	11.3	392	79.0
21.7	7.9	29.4	82.7	17.8	57.5	9.2	182	5.5	18.0	1.57	73.4	11.4	440	78.1
33.7	8.3	29.0	82.6	23.9	54.4	9.3	174	5.3	17.3	1.31	68.3	11.0	344	73.7
37.8	7.4	31.1	81.3	19.9	57.1	9.5	181	5.6	18.6	1.59	80.2	12.4	453	75.0
52.2	8.2	33.4	82.4	25.8	55.0	8.2	170	5.1	15.3	1.30	63.7	11.3	351	70.5
56.2	7.6	29.3	84.2	22.5	60.5	9.9	169	5.1	16.3	1.38	82.3	12.1	390	72.2
63.6	8.3	29.8	82.1	24.1	57.9	9.1	178	5.4	15.9	1.35	68.1	10.9	361	75.3
66	7.7	28.9	83.1	19.2	60.8	9.4	178	5.4	18.4	1.57	101.5	13.3	468	81.1
80.4	8.0	32.5	82.4	24.9	58.2	8.7	181	5.5	15.8	1.35	69.4	11.4	364	71.5
81.5	8.6	32.3	84.1	24.7	63.0	8.7	173	5.2	16.2	1.38	58.6	10.6	349	66.5
84.9	8.2	31.4	79.5	25.4	59.2	9.4	171	5.2	15.6	1.32	53.7	10.9	333	64.8
86.6	7.6	35.3	83.5	25.2	59.7	9.3	172	5.3	16.0	1.38	70.0	12.2	305	64.8
96.3	8.0	26.5	77.7	23.0	56.5	8.6	174	5.3	15.7	1.35	66.5	11.3	377	71.5
98	7.3	29.0	82.3	21.5	57.8	8.7	177	5.4	17.0	1.47	73.0	12.1	401	70.1
109	7.8	36.0	77.5	26.7	55.0	8.7	172	5.3	15.3	1.34	63.8	10.2	356	71.3
110.9	8.3	30.1	82.6	23.8	59.6	9.8	176	5.4	15.8	1.37	64.3	11.0	329	69.5
115.1	8.1	40.9	81.3	27.9	57.6	9.5	175	5.5	15.6	1.37	68.9	11.4	330	72.0
116.4	9.1	32.8	90.4	24.1	63.8	8.8	175	5.2	16.2	1.32	61.4	11.4	322	62.0
125.9	9.0	29.9	86.8	25.7	58.1	8.9	171	5.1	15.3	1.25	71.5	10.6	350	66.0
127.1	10.3	37.1	82.5	27.2	63.0	8.3	177	5.2	15.9	1.30	57.6	10.3	320	64.0
138.1	9.0	38.5	88.9	28.8	56.3	8.9	160	4.9	14.8	1.25	67.7	11.4	283	64.5
142.8	10.0	35.7	91.2	28.1	64.5	9.3	170	5.1	15.7	1.36	69.4	11.0	328	66.9
153.3	9.3	36.1	90.4	25.7	58.6	9.3	168	5.1	15.3	1.35	65.7	11.4	279	65.0
155.1	8.8	33.8	85.6	25.3	58.2	9.4	173	5.2	15.7	1.38	77.4	11.5	321	67.2
166.9	9.8	36.4	87.1	25.7	60.9	9.2	175	5.2	15.8	1.34	55.7	10.2	332	66.9
167.3	10.0	39.1	88.2	30.1	64.1	8.8	170	4.9	15.6	1.32	55.2	10.2	337	64.9
172.7	10.6	37.1	89.1	28.1	61.3	9.6	168	5.0	15.3	1.32	68.7	10.6	373	69.8
174.5	10.0	34.8	87.4	25.5	61.4	8.9	177	5.2	15.6	1.35	54.2	9.9	349	66.7
184.9	10.2	34.3	85.2	27.1	60.3	8.6	168	5.0	14.8	1.28	48.3	9.1	367	66.4
191.8	9.6	38.6	85.2	26.5	60.4	9.3	168	5.0	15.3	1.33	67.5	10.7	385	62.9
200	9.7	36.3	89.9	27.7	59.0	9.6	170	5.0	15.5	1.36	63.0	11.3	284	61.6
203.8	9.9	33.2	87.1	25.1	57.0	8.9	176	5.2	15.5	1.37	57.4	10.0	369	65.8
205	12.0	37.9	96.5	32.0	68.8	12.1	175	5.3	16.4	1.44	66.3	11.3	320	72.4
208.8	10.5	38.2	89.3	29.9	60.6	10.9	166	5.0	15.1	1.31	47.4	9.9	286	67.0
212.5	10.4	42.3	93.0	36.0	62.4	12.2	180	5.5	15.2	1.39	62.4	10.7	293	69.6
216.3	10.7	45.6	94.6	33.4	66.1	11.2	177	5.3	16.3	1.40	44.5	10.3	278	68.4
220	10.9	37.9	91.1	33.4	65.6	12.2	193	5.8	16.6	1.39	49.6	10.1	259	72.2
225	9.9	41.4	90.2	33.9	66.4	11.8	187	5.7	15.8	1.38	58.2	11.2	296	69.7
231.3	10.5	43.3	88.5	34.2	67.5	11.9	168	5.1	15.7	1.36	63.6	11.9	331	74.7
236.3	10.1	46.2	87.1	34.7	67.0	11.2	169	5.0	15.7	1.31	56.5	11.1	298	61.8
240	10.4	38.0	89.4	31.0	67.1	11.6	172	5.1	15.8	1.34	57.4	11.4	321	65.2
243.8	10.0	42.1	91.4	33.1	64.2	11.4	176	5.3	15.9	1.37	60.2	11.4	312	64.9
248.8	11.0	37.7	87.9	31.4	66.3	13.2	174	5.3	16.2	1.40	59.1	10.8	264	73.1
251.3	9.6	30.3	84.2	26.3	58.4	11.7	179	5.5	15.6	1.44	62.5	11.0	260	72.0
255	10.3	38.6	90.9	30.6	65.7	11.8	174	5.3	15.6	1.39	51.7	10.8	242	67.0
258.8	9.1	34.5	90.3	29.5	63.3	12.1	192	5.7	15.9	1.37	63.3	11.2	282	70.5
262.5	10.2	40.1	90.0	31.9	69.2	10.8	175	5.1	15.3	1.25	60.2	9.9	286	68.2
266.3	9.8	34.3	90.0	29.8	63.8	11.5	185	5.6	16.2	1.37	55.9	11.2	211	69.6
270	9.4	29.5	88.3	24.4	59.3	11.1	183	5.4	15.5	1.40	65.5	11.7	271	73.9
275	10.5	38.7	88.4	29.3	64.2	12.1	185	5.5	16.0	1.37	57.0	11.0	255	73.5
277.5	10.4	36.9	89.4	30.4	63.4	11.8	180	5.5	15.6	1.34	58.0	11.0	267	71.7
281.3	10.2	32.4	89.4	27.5	63.8	11.5	188	5.6	15.5	1.31	54.8	10.5	246	71.1
285	9.7	35.6	90.4	29.7	64.3	11.8	184	5.5	15.1	1.32	55.8	10.8	229	67.2
288.8	9.8	32.5	88.0	28.7	62.1	11.3	195	5.8	15.8	1.35	45.3	10.0	231	72.6
292.5	10.1	32.4	84.7	29.8	64.3	11.7	183	5.5	14.9	1.33	51.1	10.0	253	70.5
298.8	9.6	33.7	88.3	29.9	65.0	11.8	200	6.0	15.7	1.35	51.1	9.9	238	71.0
302.5	10.0	34.6	87.4	31.3	67.6	12.0	174	5.2	15.8	1.33	60.7	11.7	264	73.4
306.3	10.4	39.8	91.2	32.6	71.1	11.8	178	5.2	15.8	1.30	64.6	12.3	278	81.5
310	10.4	42.4	90.5	33.8	71.0	11.6	183	5.4	16.0	1.32	66.5	11.6	271	81.7
313.8	9.7	38.5	85.8	33.6	71.4	10.7	181	5.3	15.7	1.31	44.5	9.5	276	68.4
317.5	9.7	36.3	82.0	32.0	67.7	11.5	203	6.1	15.8	1.34	66.4	10.5	303	77.5
321.3	10.3	41.8	84.1	31.3	67.4	11.2	196	5.8	15.7	1.33	70.7	10.5	315	76.5

silicate fraction analyzed in the present study, Cr is incorporated into silicate minerals, mainly augite, hornblende, and magnesian olivine. Cu and Zn also show similar geochemical behaviors: in silicates, Cu and Zn may replace Fe^{2+} and Mg^{2+} to a limited extent, and these elements are found at much higher concentrations in basic rocks than in acidic rocks. Therefore, the observed decrease in concentrations of Co, Ni, Cr, Cu, and Zn reflects a change in the detrital source, which can be explained by their dilution due to an increase in the contribution of felsic rocks.

Pb concentrations show a remarkable decline after 2.6 Ma (Fig. 4). In sedimentary rocks, Pb exists mainly in resistates and clay minerals. Therefore, the measured decrease in Pb concentrations is thought to be related mainly to less-intense weathering of continental source rocks.

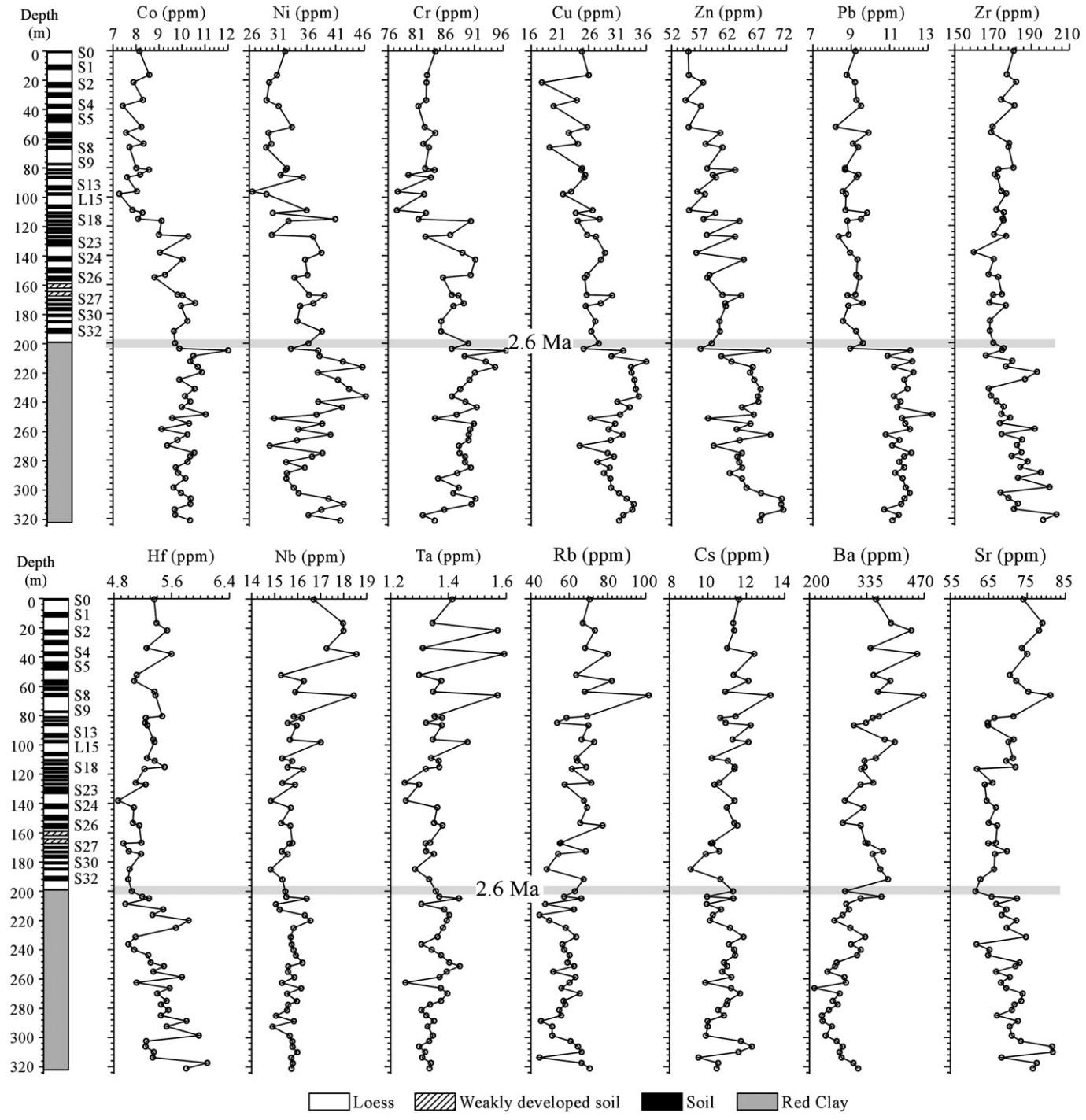

Fig. 4. Vertical variations in trace element concentrations within the Jingchuan section.

Zr and Hf have similar geochemical properties. The Zr content of sedimentary rocks is strongly related to the presence of detrital heavy minerals such as zircon and sphene. Zr is highly resistant to chemical weathering, making it useful for geochemical tracing. Felsic igneous rocks are generally enriched in Zr and Hf relative to mafic rocks (Mielke, 1979). Accordingly, the decreasing trend in Zr and Hf concentrations observed after 2.6 Ma in the present study mainly reflects a change in the parent rock types and/or less-intensive weathering of the source region.

Nb and Ta have similar physical and chemical properties: both are high field strength elements, have limited solubility in water, and are generally considered immobile (Kurtz et al., 2000; Little and Lee, 2006). Therefore, the increasing trends in Nb and Ta observed in the present study are thought to reflect provenance change.

Rb and Cs are alkali metals, while Sr and Ba are alkaline earth metals. In the present study, vertical variations in these elements are generally characterized by an increasing trend after 2.6 Ma (Fig. 4). In silicate minerals, Rb, Cs, and Ba are hosted in K-bearing minerals, mainly micas and feldspars (Mielke, 1979; Muhs et al., 2003). The contents of Rb, Cs, and Ba show a marked increase from mafic to felsic rocks. The observed increase in the concentrations of these elements in Quaternary eolian dust indicates a trend towards a higher proportion of felsic rocks in the source area. The geochemical behavior of Sr follows that of Ca. In the silicate fraction analyzed in the present study, Sr is hosted mainly in Ca-plagioclase, indicating a marked increase in the content of Ca-plagioclase in the source rocks of Quaternary eolian deposits.

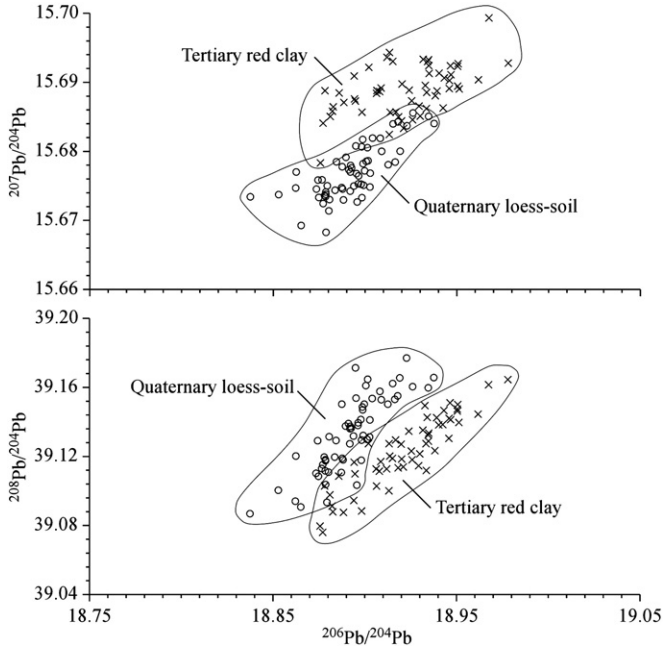

Fig. 5. Plots of $^{207}Pb/^{204}Pb$ versus $^{206}Pb/^{204}Pb$ and $^{208}Pb/^{204}Pb$ versus $^{206}Pb/^{204}Pb$ for samples of late Tertiary Red Clay and Quaternary eolian deposits.

Although pre- and post-deposition chemical weathering of eolian deposits may affect the trace element composition, the following lines of evidence indicate that the influence of such weathering was largely negligible in the present study. First, because Rb and Ba are relatively concentrated in weathered residue compared with Sr, values of Rb/Sr and Ba/Sr are high in strongly weathered soils, and these ratios are used as indices of chemical weathering (Retallack, 1994; Gallet et al., 1996; Chen et al., 1999). In the present study, however, vertical variations in both Rb/Sr and Ba/Sr show an increasing trend after 2.6 Ma (Fig. 7), in contrast to the climatic cooling trend observed from

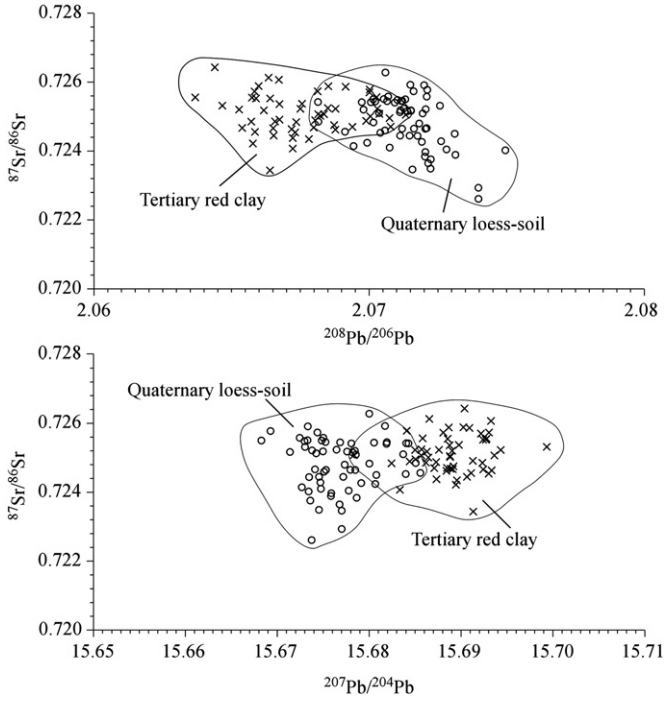

Fig. 6. Plots of $^{87}Sr/^{86}Sr$ versus $^{208}Pb/^{206}Pb$ and $^{87}Sr/^{86}Sr$ versus $^{207}Pb/^{204}Pb$ for samples of late Tertiary Red Clay and Quaternary eolian deposits (Sr isotope data are from Sun, 2005).

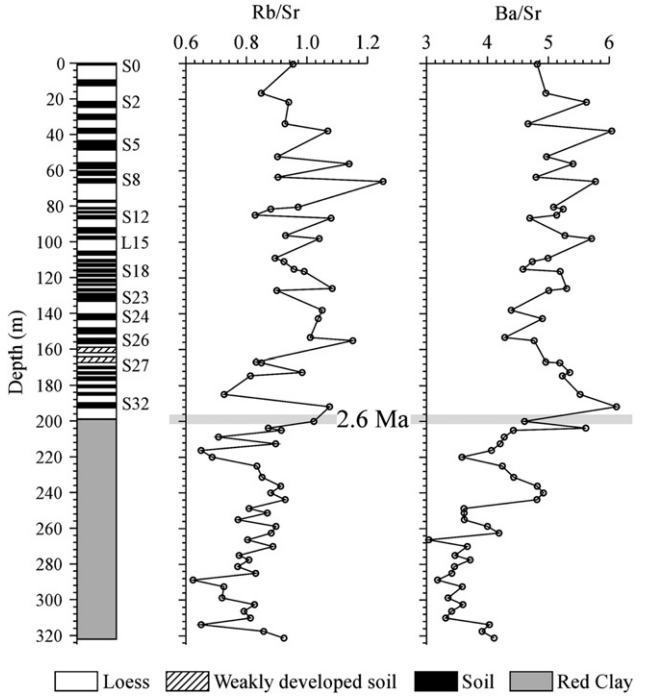

Fig. 7. Temporal variations in Rb/Sr and Ba/Sr for the silicate fraction, showing increasing trends after 2.6 Ma.

the late Cenozoic. This finding demonstrates that the trace element composition of the silicate fraction at Jingchuan reflects the nature of the source rocks rather than chemical weathering.

Second, the degree of chemical weathering can be quantified by the chemical index of alteration (CIA), as proposed by Nesbitt and Young (1982): $CIA = (Al_2O_3/(Al_2O_3 + CaO^* + Na_2O + K_2O) \times 100$. High CIA values indicate strong chemical alteration. In this study, we calculated CIA values based on major element data (Suppl. Table 1). Nesbitt et al. (1980) examined the distribution of alkali and alkaline earth elements in a weathering profile and noted that larger cations (e.g., Rb and Cs) are fixed in weathering profiles as a result of ion-exchange processes, whereas smaller cations (e.g., Na and Ca) are lost in solution. In the present study, Fig. 8 shows a general decreasing trend of Rb and Cs concentrations with enhanced chemical weathering, which is inconsistent with the hypothesis that chemical weathering played an important role in governing the chemical composition of the fine silicate fraction at Jingchuan. This finding provides further evidence that the composition of the silicate fraction at Jingchuan reflects mainly provenance information rather than chemical weathering.

4.3. Mechanism of the change in eolian dust provenance at 2.6 Ma

Although the Gobi and sand deserts in southern Mongolia and adjoining regions in China are regarded as the main source areas of Quaternary airborne dust found upon the Loess Plateau, these areas serve as dust reservoirs rather than dust producers (Sun, 2002). In China, a desert origin of loess-sized material was proposed in the pioneering work of Obruchev (1911). However, Smalley and Vita-Finzi (1968) argued that no specific desert process is able to produce the vast amounts of silt required to form a large loess deposit. Smalley (1966) argued that glacial grinding is an efficient producer of loess-size material. Indeed, Sun (2002) demonstrated that glacial grinding and frost weathering played an important role in the production of Quaternary eolian deposits upon the Loess Plateau. In this context, Quaternary mountain glaciers are likely to have influenced the provenance of dust by dominating the production of loess-sized material.

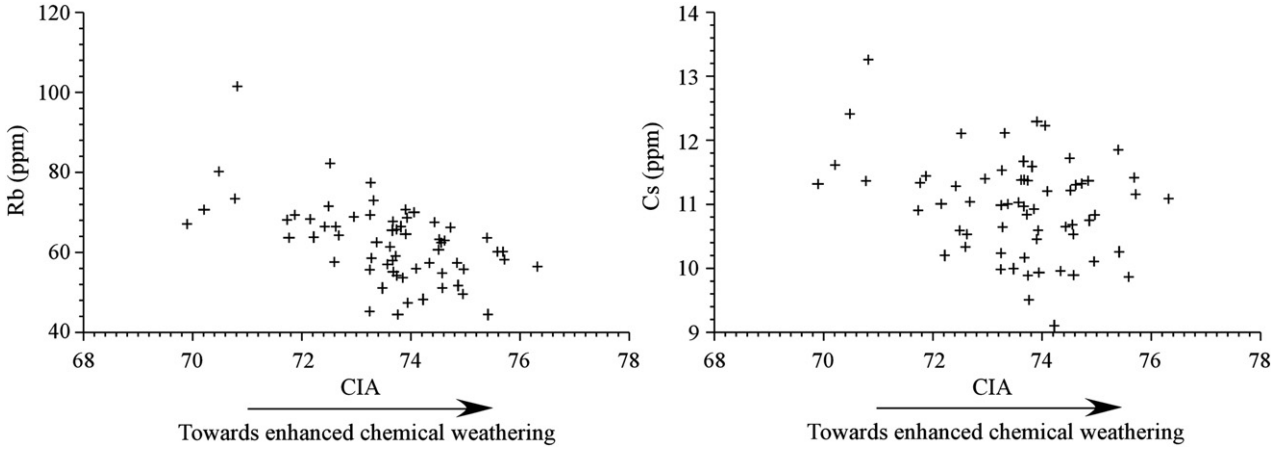

Fig. 8. Contents of Rb and Cs versus the chemical index of alteration (CIA), showing that the concentrations of the two elements do not increase with intensified chemical weathering.

On the Loess Plateau, the boundary between the reddish Red Clay and overlying yellowish-brownish loess–soil succession occurs at around 2.6 Ma. Moreover, deep sea records of ice-rafted debris (IRD) indicate that although the first major pulse of debris occurred at 3.3 Ma, suggesting a marked expansion of the Greenland ice sheet, the synchronous development of ice sheets in Greenland, Scandinavia, and North America started at 2.6–2.7 Ma (Kleiven et al., 2002). The high mountains in Central Asia are located in mid-latitude regions, and were under a relatively warm climate during the late Tertiary, unsuitable for the development of mountain glaciers in the dust-source regions of northwest China, as indicated by a lack of late Tertiary glacial moraines (Fig. 9a). Therefore, the amount of dust and slit produced from surrounding mountains was limited compared with that during the Quaternary, when Pleistocene glaciation prevailed (Fig. 9b).

Since 2.6 Ma, Pleistocene mountain glaciers have become established on the high mountains of northwestern China (Fig. 9b), as indicated by the occurrence of glacial moraine (Zhang, 1985). The accompanying glacial erosion would have produced a tremendous amount of loess-sized material that was ultimately outwashed to the piedmont plains and was then sorted by wind. Moreover, because glacial grinding and frost weathering occur in areas at high elevations, such alpine processes generate more material from areas of high topographic relief (Fig. 9b). In this context, the Quaternary eolian deposits contain a higher proportion of material from areas of high relief and less material from low-lying regions compared with the Tertiary Red Clay.

5. Conclusions

Based on temporal variations in Pb isotopes and trace element concentrations within airborne dust on the central Loess Plateau, we got the following conclusions.

(1) In contrast to the composition of bulk samples, which is related to both provenance change and chemical weathering, the silicate fraction of eolian dust on the Loess Plateau reflects mainly the geochemical characteristics of the source material.

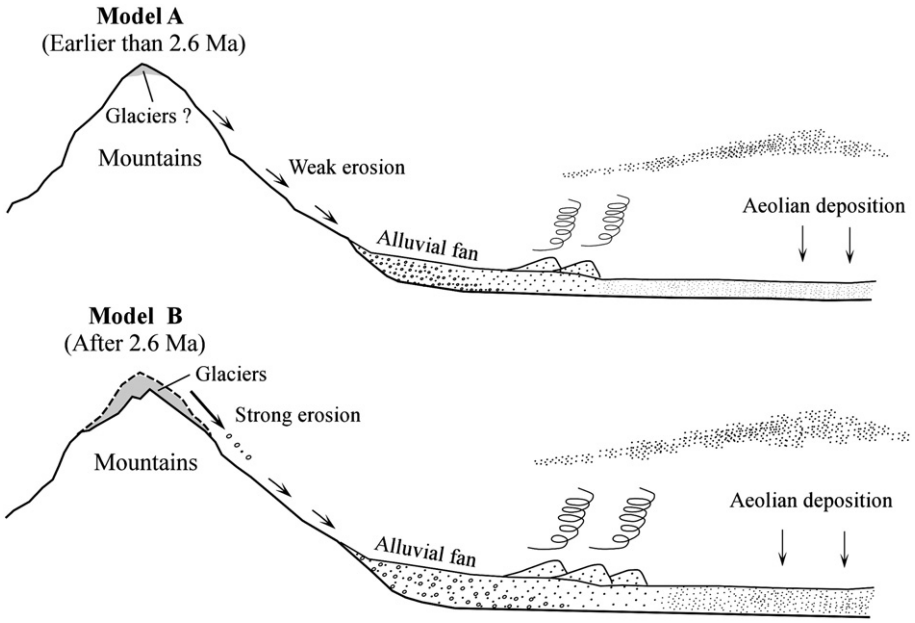

Fig. 9. Conceptual models of the production, transportation, and deposition of dust in northwestern China. (a) During the late Tertiary (before 2.6 Ma), the warm climate did not favor the development of mountain glaciers in mid-latitude mountains, resulting in low rates of denudation, limited production fine dust, and low rates of dust deposition. (b) During the time of Pleistocene glaciation (after 2.6 Ma), the occurrence of glacial grinding resulted in accelerated rock denudation, with the result that coarse debris from high elevations became the dominant source material for Quaternary loess.

(2) Vertical variations in Pb isotopes and trace element concentrations show distinct changes after 2.6 Ma, related mainly to changes in the source of the dust.
(3) The change in the source of eolian dust at 2.6 Ma is coincident with the initiation of Quaternary glaciation in the Northern Hemisphere. The dramatic climatic cooling induced glacial grinding, which played an important role in modifying the source material of the dust.
(4) Temporal changes in trace element compositions demonstrate that the source material became increasingly dominated by felsic rocks after 2.6 Ma. Because Quaternary glacial grinding occurred in areas at high elevations, eolian dust produced during this time tended to be derived from mainly high mountainous areas rather than low-lying cratonic regions.

Acknowledgements

This work was supported by Projects KZCX2-YW-130 and KZCX2-YW-Q09-06-04 of the Chinese Academy of Sciences, and the National Nature Science Foundation of China (grants 40830104, 40772115, and 40331005). We thank Dr. S.L. Yang for providing samples of Quaternary loess and soil, and X.D. Jin for assistance with performing the experiments.

Appendix A. Supplementary data

Supplementary data associated with this article can be found, in the online version, at doi:10.1016/j.epsl.2010.01.001.

References

Asahara, Y., 1999. Provenance of the north Pacific sediments and process of source material transport as derived from Rb-Sr isotopic systematics. Chem. Geol. 158, 271–291.
Belshawa, N.S., Freedmanb, P.A., O'Nionsa, R.K., Franka, M., Guo, Y., 1998. A new variable dispersion double-focusing plasma mass spectrometer with performance illustrated for Pb isotopes. Int. J. Mass Spectrom. 181, 51–58.
Biscaye, P.E., Grousset, F.E., Revel, M., VanderGaast, S., Zielinski, G.A., Vaars, A., Kukla, G., 1997. Asian provenance of glacial dust (stage 2) in the Greenland Ice Sheet Project 2 Ice Core, Summit, Greenland. J. Geophys. Res. 102, 26,765–26,780.
Chen, J., An, Z.S., Head, J., 1999. Variation of Rb/Sr ratios in the loess–paleosol sequences of central China during the last 130, 000 years and their implications for monsoon paleoclimatology. Quat. Res. 51, 215–219.
Derbyshire, E., Meng, X.M., Kemp, R.A., 1998. Provenance, transport and characteristics of modern eolian dust in western Gansu Province, China, and interpretation of the Quaternary loess record. J. Arid Environ. 39, 497–516.
Ding, Z.L., Yu, Z.W., Rutter, N.W., Liu, T.S., 1994. Towards an orbital time scale for Chinese loess deposits. Quat. Sci. Rev. 13, 39–70.
Ding, Z.L., Yang, S.L., Hou, S.S., Wang, X., Chen, Z., Liu, T.S., 2001a. Magnetostratigraphy and sedimentology of the Jingchuan red clay section and correlation of the Tertiary eolian red clay sediments of the Chinese Loess Plateau. J. Geophys. Res. 106, 6399–6408.
Ding, Z.L., Sun, J.M., Yang, S.L., Liu, T.S., 2001b. Geochemistry of the Pliocene red clay formation in the Chinese Loess Plateau and implications for its origin, source provenance and paleoclimate change. Geochim. Cosmochim. Acta 65, 901–913.
Gallet, S., Jahn, B.M., Torii, M., 1996. Geochemical characterization of the Luochuan loess–paleosol sequence, China, and paleoclimatic implications. Chem. Geol. 133, 67–88.
Godfrey, L.V., 2002. Temporal changes in the lead isotopic composition of red clays: comparison with ferromanganese crust records. Chem. Geol. 185, 241–254.
Guo, Z.T., Fedoroff, N., 1991. Paleoclimatic and stratigraphic implications of the paleosol S1 in the loess sequence in China. In: Liu, T.S. (Ed.), Loess, Environment and Global Change. Science Press, Beijing, pp. 187–198.
Heller, F., Liu, T.S., 1984. Magnetism of Chinese loess deposits. Geophys. J. R. Astron. Soc. 77, 125–141.
Ji, J.F., Chen, J., Balsam, W., Lu, H.Y., Sun, Y.B., Xu, H.F., 2004. High resolution hematite/goethite records from Chinese loess sequences for the last glacial–interglacial cycle: rapid climatic response of the East Asian Monsoon to the tropical Pacific. Geophys. Res. Lett. 31, L03207. doi:10.1029/2003GL018975.
Jones, C.E., Halliday, A.N., Rea, D.K., Owen, R.M., 2000. Eolian inputs of lead to the North Pacific. Geochim. Cosmochim. Acta 64, 1405–1416.
Kleiven, H.F., Jansen, E., Fronval, T., Smith, T.M., 2002. Intensification of Northern Hemisphere glaciations in the circum Atlantic region (3.5–2.4 Ma) — ice-rafted detritus evidence. Palaeogeogr. Palaeoclimatol. Palaeoecol. 184, 213–223.
Klemm, V., Reynolds, B., Frank, M., Pettke, T., Halliday, A.N., 2007. Cenozoic changes in atmospheric lead recorded in central Pacific ferromanganese crusts. Earth Planet. Sci. Lett. 253, 57–66.
Kukla, G., An, Z.S., 1989. Loess stratigraphy in central China. Palaeogeogr. Palaeoclimat. Palaeoecol. 72, 203–255.
Kurtz, A.C., Derry, L.A., Chadwick, O.A., Alfano, M.J., 2000. Refractory element mobility in volcanic soils. Geology 28, 683–686.
Little, M.G., Lee, C.-T.A., 2006. On the formation of an inverted weathering profile on Mount Kilimanjaro, Tanzania: buried paleosol or groundwater weathering? Chem. Geol. 235, 205–221.
Liu, T.S., 1985. Loess and the Environment. China Ocean Press, Beijing. 251 pp.
Liu, T.S., Gu, X.F., An, Z.S., Fan, Y.X., 1981. The dust fall in Beijing, China on April 18, 1980. Geol. Soc. Am. Special Paper 186, 149–157.
Mielke, J.E., 1979. Composition of the Earth's crust and distribution of the elements. In: Siegel, F.R. (Ed.), Review of Research on Modern Problems in Geochemistry. UNESCO Report, Paris, pp. 13–37.
Muhs, D.R., Ager, T.A., Bettis III, E.A., McGeehin, J., Been, J.M., Begét, J.E., Pavich, M.J., Stafford Jr., T.W., Stevens, D.A.S.P., 2003. Stratigraphy and palaeoclimatic significance of Late Quaternary loess–palaeosol sequences of the Last Interglacial–Glacial cycle in central Alaska. Quart. Sci. Rev. 22, 1947–1986.
Nesbitt, H.W., Young, G.M., 1982. Early Proterozoic climates and plate motions inferred from major element chemistry of lutites. Nature 299, 715–717.
Nesbitt, H.W., Markovics, G., Price, R.C., 1980. Chemical processes affecting alkalies and alkaline earths during continental weathering. Geochim. Cosmochim. Acta 44, 1659–1666.
Obruchev, V.A., 1911. The question of the origin of loess — in defence of the eolian hypothesis. Izvêstiya Tomskago Tekhnologicheskago Instituta 33, 38.
Pettke, T., Halliday, A.N., Hall, C.M., Rea, D.K., 2000. Dust production and deposition in Asia and the north Pacific Ocean over the past 12 Myr. Earth Planet. Sci. Lett. 178, 397–413.
Pye, K., 1987. Eolian Dust and Dust Deposits. Academic Press, London. 334 pp.
Retallack, G.J., 1994. A pedotype approach to latest Cretaceous and earliest Tertiary paleosols in eastern Montana. Geol. Soc. Am. Bull. 106, 1377–1397.
Schettler, G., Romer, R.L., Qiang, M.R., Plessen, B., Dulski, P., 2009. Size-dependent geochemical signatures of Holocene loess deposits from the Hexi Corridor (China). J. Asian Earth Sci. 35, 103–136.
Smalley, I.J., 1966. The properties of glacial loess and formation of loess deposits. J. Sediment. Petrol. 36, 669–676.
Smalley, I.J., Vita-Finzi, C., 1968. The formation of fine particles in sand deserts and the nature of "desert" loess. J. Sediment. Petrol. 38, 766–774.
Stancin, A., Gleason, J.D., Rea, D.K., Owen, R.M., Moore Jr., T.C., Blum, J.D., Hovan, S.A., 2006. Radiogenic isotope mapping of late Cenozoic eolian and hemipelagic sediment distribution in the east-central Pacific. Earth Planet. Sci. Lett. 248, 840–850.
Sun, J.M., 2002. Provenance of loess material and formation of loess deposits on the Chinese Loess Plateau. Earth Planet. Sci. Lett. 203, 845–859.
Sun, J.M., 2005. Nd and Sr isotopic variations in Chinese eolian deposits during the past 8 Ma: implications for provenance change. Earth Planet. Sci. Lett. 240, 454–466.
Sun, J.M., Liu, T.S., Lei, Z.F., 2000. Source regions of heavy dust fall in Beijing, China on April 16, 1998. Geophys. Res. Lett. 27, 2105–2108.
Sun, J.M., Zhang, M.Y., Liu, T.S., 2001. Spatial and temporal characteristics of dust storms in China and its surrounding regions, 1960–1999: relations to source area and climate. J. Geophys. Res. (D-series) 106, 10,325–10,334.
van de Flierdt, T., Frank, M., Halliday, A.N., Hein, J.R., Hattendorf, B., Günther, D., Kubik, P.W., 2003. Lead isotopes in North Pacific deep water — implications for past changes in input sources and circulation patterns. Earth Planet. Sci. Lett. 209, 149–164.
Zhang, H.Y., 1985. Quaternary glaciation in the northern Tianshan. In: Mao, D.H., Yang, Z.X., Zhou, C.J., Li, J.F., Xia, X.C., Wang, S.J., Peng, X.L., Hong, L., Han, S.T., Zhang, H.Y. (Eds.), Proceedings of Quaternary Research of Arid Xinjiang. Xinjiang Renmin Press, Urumuqi, pp. 55–68.
Zhu, X.K., O'Nions, R.K., Belshaw, N.S., Guo, Y., 1988. Provenance shifts of Chinese loess monitored by Pb isotopes. Chin. Sci. Bull. 43, 166.